https://doi.org/10.1093/plphys/kiad052 PLANT PHYSIOLOGY 2023: 192: 356–369

Plant Physiology®

Research Article

Manganese concentration affects chloroplast structure and the photosynthetic apparatus in *Marchantia polymorpha*

Marine Messant,[1] Umama Hani,[1] Thaïs Hennebelle,[1] Florence Guérard,[2] Bertrand Gakière,[2] Andrew Gall,[1] Sébastien Thomine[1] and Anja Krieger-Liszkay[1,*]

1 Institute for Integrative Biology of the Cell (I2BC), CEA, CNRS, Université Paris-Saclay, 91198 Gif-sur-Yvette cedex, France
2 Institute of Plant Sciences Paris-Saclay, CNRS, Université Paris-Sud, Institut National de la Recherche Agronomique, Université d'Evry, Université Paris-Diderot, Université Paris-Saclay, 91405 Orsay Cedex, France

*Author for correspondence: anja.liszkay@i2bc.paris-saclay.fr (A.K.-L.)
The author responsible for distribution of materials integral to the findings presented in this article in accordance with the policy described in the Instructions for Authors (https://academic.oup.com/plphys/pages/General-Instructions) is A.K.-L. (anja.liszkay@i2bc.paris-saclay.fr).

Abstract

Manganese (Mn) is an essential metal for plant growth. The most important Mn-containing enzyme is the Mn_4CaO_5 cluster that catalyzes water oxidation in photosystem II (PSII). Mn deficiency primarily affects photosynthesis, whereas Mn excess is generally toxic. Here, we studied Mn excess and deficiency in the liverwort *Marchantia polymorpha*, an emerging model ideally suited for analysis of metal stress since it accumulates rapidly toxic substances due to the absence of well-developed vascular and radicular systems and a reduced cuticle. We established growth conditions for Mn excess and deficiency and analyzed the metal content in thalli and isolated chloroplasts. In vivo super-resolution fluorescence microscopy and transmission electron microscopy revealed changes in the organization of the thylakoid membrane under Mn excess and deficiency. Both Mn excess and Mn deficiency increased the stacking of the thylakoid membrane. We investigated photosynthetic performance by measuring chlorophyll fluorescence at room temperature and 77 K, measuring P700 absorbance, and studying the susceptibility of thalli to photoinhibition. Nonoptimal Mn concentrations changed the ratio of PSI to PSII. Upon Mn deficiency, higher non-photochemical quenching was observed, electron donation to PSI was favored, and PSII was less susceptible to photoinhibition. Mn deficiency seemed to favor cyclic electron flow around PSI, thereby protecting PSII in high light. The results presented here suggest an important role of Mn in the organization of the thylakoid membrane and photosynthetic electron transport.

Introduction

Manganese (Mn) is an essential element for plant growth. Mn homeostasis is disturbed under suboptimal or excessive Mn availability (Schmidt et al. 2016; Alejandro et al. 2020). The most important Mn-containing enzyme is the Mn_4CaO_5 cluster at photosystem II (PSII) that catalyzes water oxidation. Although Mn is involved as a cofactor in a range of biochemical pathways, the primary effect of Mn deficiency in photosynthetic organisms is a decrease in photosynthetic activity (Marschner 1995). Furthermore, Mn is involved in reactive oxygen species (ROS) metabolism and in the antioxidant response. Manganese is the cofactor of the manganese superoxide dismutase (MnSOD) found in mitochondria and peroxisomes (Bowler et al. 1994; Corpas et al. 2017). Oxalate oxidase (OxOx) present in the apoplast also requires Mn. This enzyme catalyzes the oxidation of oxalate to carbon dioxide coupled with the reduction of oxygen to hydrogen peroxide (Requena and Bornemann 1999), the latter having an essential role in the defense against pathogens (Lane 2002). When accumulated in excess, Mn can be toxic causing oxidative stress (Marschner 1995; Pittman 2005; Delhaize et al. 2007; Peiter et al. 2007; Eroglu et al. 2016).

Received September 9, 2022. Accepted December 6, 2022. Advance access publication February 1, 2023

In the presence of excess Mn in the soil, there is a competition between the uptake of Mn and other metals that are also essential for the plant (Alam et al. 2005; St. Clair and Lynch, 2005; Blamey et al. 2015; Lešková et al. 2017). Indeed, at the level of the roots, plants do not have transporters that are completely selective for a single metal. Thus, a high abundance of Mn can lead to a decrease in the absorption of other essential metals such as calcium, magnesium, iron, or even phosphorus, thereby negatively affecting photosynthesis (Nable et al. 1988; Amao and Ohashi 2008) and inhibiting chlorophyll synthesis (Clairmont et al. 1986; Subrahmanyam and Rathore 2001). Manganese excess causes chlorosis followed by necrosis leading to plant death, but these symptoms are very variable and species dependent (Millaleo et al. 2010). To overcome Mn toxicity, plants have developed different ways of Mn storage in vacuoles (Ducic and Polle 2007), cell walls (Führs et al. 2010), and even Golgi vesicles (Marschner 1995; Pittman 2005). In the literature, plant species have been divided into tolerant and non-tolerant to Mn excess. Some species can hyperaccumulate Mn at levels above 10,000 $mg.kg^{-1}$ dry weight (DW) (Van der Ent et al. 2013).

The effect of Mn deficiency on photosynthetic electron transport and chloroplast structure has been studied for decades in a number of different organisms ranging from cyanobacteria to angiosperms (e.g. Homann 1967; Salomon and Keren 2011). In general, a decline in PSII activity is observed although symptoms of Mn deficiency are species dependent (Homann 1967). Depending on the severity of Mn deficiency, the ultrastructure of chloroplasts may be perturbed. In slightly Mn-deficient spinach (*Spinacia oleracea*) plants, the stroma lamellae are affected, while the grana stacks are normal. Under more severe Mn deficiency, grana stacks are also disorganized (Mercer et al. 1962). More recently, similar observations were reported in the Arabidopsis (*Arabidopsis thaliana*) knockout mutant chloroplast Mn transporter1 (CMT1), a transporter localized in the inner envelope membrane, where chloroplast development was abnormal and thylakoids appeared disorganized, with either hypo- or hyper-stacked grana lamellae (Eisenhut et al. 2018; Zhang et al. 2018). In this mutant, a large heterogeneity between the chloroplasts was observed with chloroplasts containing a well-structured, normal organization of the thylakoid membranes next to chloroplasts with completely disorganized architectures (Eisenhut et al. 2018). The consequences of the loss of PSII activity and the disorganization of the thylakoid membrane on the ratio of linear and cyclic photosynthetic electron transport have not been investigated in previous studies.

In this present study, we investigated the consequences of both excess and deficiency of Mn on photosynthesis in the liverwort *Marchantia polymorpha*, an emerging model system. Marchantia has been described in the 1990s as being able to hyperaccumulate certain metals such as, for example, lead (Samecka-Cymerman et al. 1997). Due to the morphology of the thalli, the ventral part and hyaline parenchyma of the plant are in direct contact with the substrate allowing the uptake of the metals from the medium without having to pass through the root system as occurs in vascular plants. Compared to vascular plants, the leaf anatomy of Marchantia is simpler and the tissues are thinner. Chloroplasts are less structured than in vascular plants (Tanaka et al. 2017) with smaller grana stacks, making these chloroplasts an ideal system for super-resolution fluorescence microscopy.

We have established conditions for cultivating Marchantia on plates under Mn deficiency and excess. The metal content, metabolome, and antioxidant activities as well as photosynthetic activity and chloroplast structure were determined to investigate the response of Marchantia to non-optimal Mn supply. Manganese excess and deficiency affect these processes in different ways. Manganese excess led to a strong response of the metabolome but subtle defects in photosynthesis, whereas, in contrast, Mn deficiency affected the activity of PSII and promoted cyclic electron transport around PSI. Under Mn deficiency, an increase in non-photochemical fluorescence quenching was observed, protecting PSII against photoinhibition.

Results

Part I: Mn excess induces a stress response and affects the photosynthetic apparatus

In order to determine the effect of Mn excess on *M. polymorpha*, plants were cultivated on media containing different $MnCl_2$ concentrations, ranging from 33 µM (Agar Control) to 6.5 mM (200×) manganese. Gemmae were cultured on a standard Gamborg's B5 medium (33 µM $MnCl_2$) for 2 weeks before being transferred for 1 week to the different Mn concentrations before analysis. Figure 1A shows that thalli were able to grow normally up to 1 mM Mn. However, thalli showed reduced growth from 2 up to 6.6 mM Mn, with signs of stress visible as brown spots. The chlorophyll content of the thalli was significantly decreased in excess Mn conditions (SI Table 1). The determination of Mn concentration in thalli (Figure 1B) showed that there is a positive correlation between Mn accumulation and Mn concentration in the medium. In addition to Mn, we determined Fe and Mg content since high Mn may negatively impact Fe import into the chloroplasts and thereby the assembly of FeS clusters in PSI (Millaleo et al. 2013), and Mg is important for stacking of the thylakoid membranes. Neither Fe nor Mg content was affected by the high Mn concentrations.

In the following, we focus on the conditions of Mn excess 30 × and 200 ×. The first being the highest concentration at which Marchantia showed no obvious signs of stress and the second being the most stressful condition. We conducted a metabolomic analysis by gas chromatography–mass spectrometry (GC-MS) on thalli. In total, 94 metabolites have been identified and quantified (Supplemental Figure S1, Tables S2 and S3). Regarding the

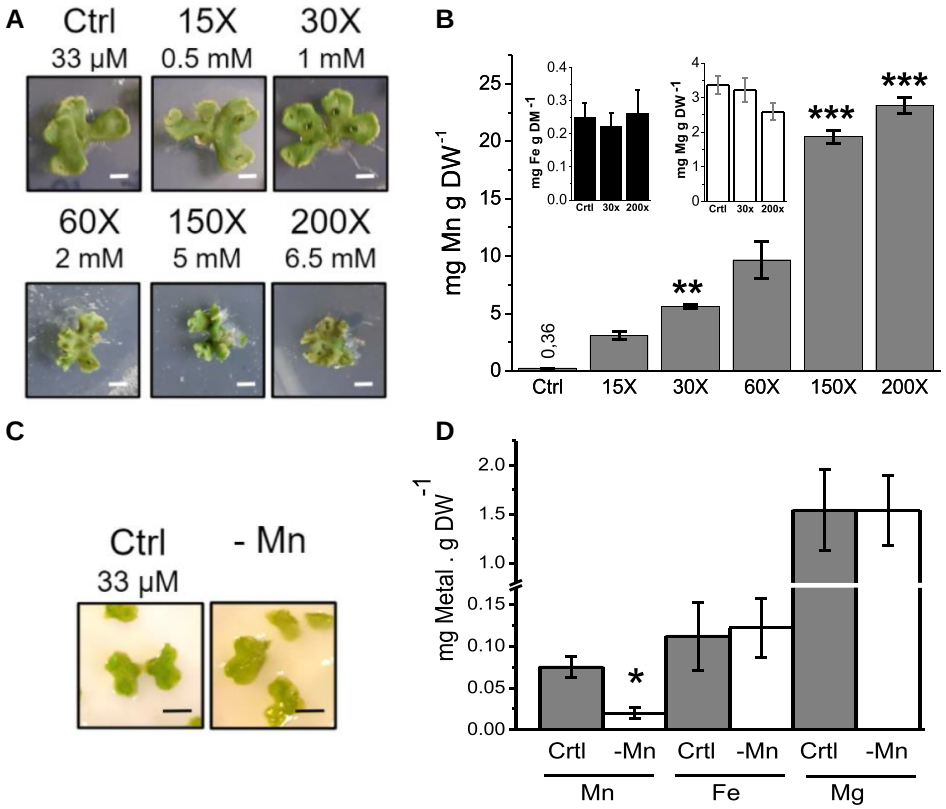

Figure 1. Effect of nonoptimal Mn supply on growth and metal content of *Marchantia polymorpha*. Mn excess: **A)** 2-wk-old thalli were transferred for 1 week to agar plates containing 33 µM (control, Crtl), 0.5 mM (15×), 1 mM (30×), 2 mM (60×), 5 mM (150×), and 6.5 mM (200×) $MnCl_2$, respectively. White scale bars represent 1 cm. **B)** Manganese, iron, and magnesium concentrations were determined after 1-week growth with the given Mn concentrations. Mn deficiency: **C)** 2-week-old thalli were transferred and grown for 1 week on starch plates with or without the addition of 33 µM $MnCl_2$. Black scale bars represent 1 cm. **D)** Manganese, iron, and magnesium concentrations in thalli were measured after 1 week of growth on starch plates with (Ctrl, hatched bars) or without $MnCl_2$ (-Mn, white bars) in the medium. Error bars in **B** and **D** represent standard errors. Stars in **B** and **D** indicate significant differences, compared to the control condition, based on a Mann–Whitney test (*$P < 0.05$, **$P < 0.01$, ***$P < 0.001$; $N \geq 3$ biological replicates).

200× condition, certain metabolites involved in the response to heavy metal or oxidative stresses were strongly increased, while all other metabolites decreased compared to the control. A very high concentration of Mn was associated with a strong induction of polyamine synthesis with an accumulation of ornithine, citrulline, and putrescine (Table 1). Among sugars and their derivatives, strong increases in trehalose, rhamnose, and galacturonic acid were also observed. All these compounds are known to accumulate in plants and other organisms upon exposure to heavy metals (Sharma and Dietz 2006; Singh et al. 2016; Liu et al. 2017; Hasanuzzaman et al. 2019; Alejandro et al. 2020). Most striking, *N*-methylalanine content was 30 and 50 times higher in 30× and 200× conditions, respectively. To further investigate the response to oxidative stress, the activity of a few antioxidant enzymes was measured (Table 2). A 2-fold increase in superoxide dismutase (SOD) activity was observed at the highest Mn concentration. The activity of class III peroxidases was also slightly increased at 200×, while catalase activity gradually decreased.

Table 1. Increase in metabolites involved in oxidative stress response upon growth on high Mn concentration

Metabolite	Experimental condition		
	Ctrl	30×	200×
Citrulline	0.001 ± 0	0.001 ± 0	0.003 ± 0.001
Galacturonic acid	0.004 ± 0	0.004 ± 0.001	0.008 ± 0.001
L-ornithine	0.003 ± 0.001	0.003 ± 0	0.007 ± 0.001
N-Methylalanine	0.021 ± 0.002	0.67 ± 0.237	1.101 ± 0.038
Putrescine	0.003 ± 0.001	0.002 ± 0	0.008 ± 0.001
Rhamnose	0.004 ± 0	0.004 ± 0.001	0.008 ± 0.001
Trehalose	0.053 ± 0.003	0.049 ± 0.008	0.083 ± 0.012

List of selected metabolites showing an increase in plants grown in 200× condition. The mean value and SD are given ($N = 4$). $P < 0.05$ for all values, according to the 2-way ANOVA test. See Supplemental Table S2 for the full list.

Next, we studied the impact of Mn excess on chloroplast ultrastructure and photosynthetic activity. The concentration of Mn, Fe, and Mg was measured in isolated intact chloroplasts (Figure 2A). The results show a gradual and significant increase of Mn comparable with the observation made in the

Table 2. Antioxidant enzymes activities in thalli from control and manganese excess and deficiency conditions

Parameter	Experimental condition				
	Ctrl	30×	200×	Starch + Mn	Starch − Mn
SOD activity	3.01 ± 0.63	4.19** ± 0.86	6.00*** ± 1.48	5.63 ± 1.43	5.08 ± 0.63
CAT activity	1.18 ± 0.16	0.87** ± 0.26	0.54*** ± 0.12	0.72 ± 0.16	0.70 ± 0.13
PRX activity	1.27 ± 0.38	1.17 ± 0.25	1.59* ± 0.42	1.52 ± 0.20	1.04** ± 0.40
ROS	—	—	—	44.4 ± 4.2	100 ± 1.4

Superoxide dismutase, Catalase, and peroxidase activities (µmol substrate mg proteins^{-1} min^{-1}) were measured in crude extracts. $^{\bullet}OH$ derived from $H_2O_2/O_2^{\bullet-}$ was measured using electron paramagnetic resonance (EPR) as a hydroxyethyl-*N*-tert-butyl-α-(4-pyridyl)nitrone *N*′-oxide.
(4-POBN) adduct. Mean value and SD are given. Stars indicate a significant difference compared to the control condition, based on a Mann–Whitney test (*$P < 0.01$, **$P < 0.01$, ***$P < 0.001$, $N = 3$ biological replicates).

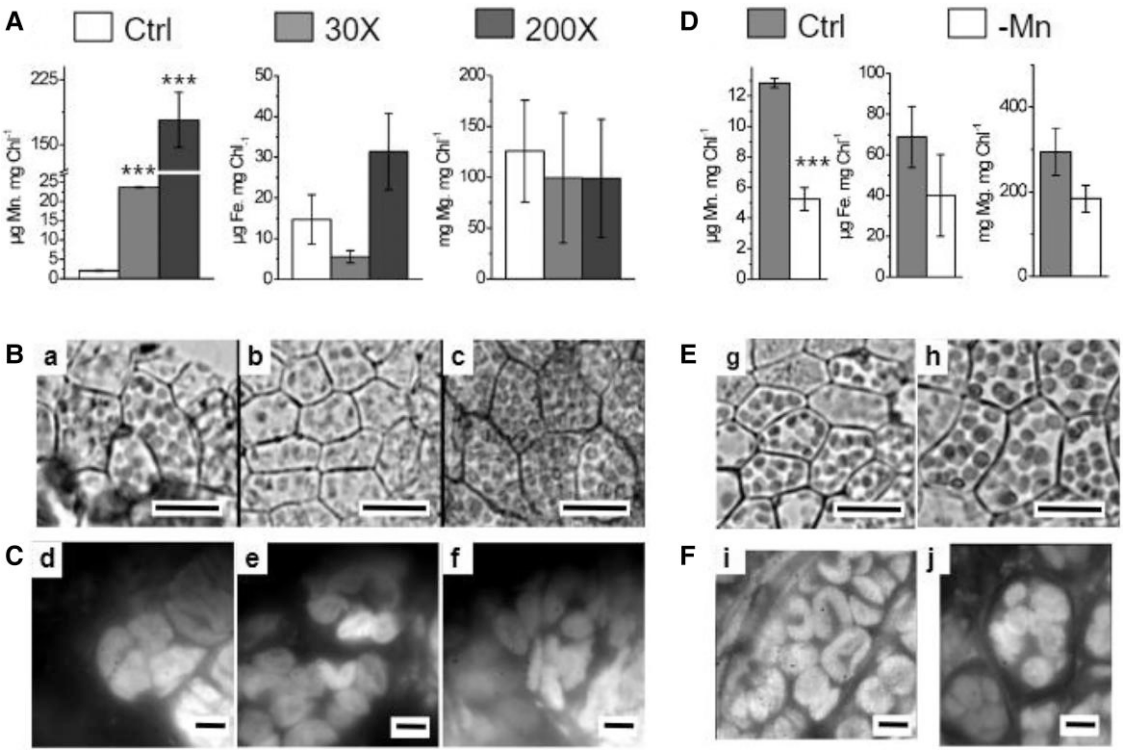

Figure 2. Chloroplast metal content and structure in *Marchantia polymorpha* grown on nonoptimal Mn supply. Mn excess: **A)** Metal content of intact chloroplasts isolated from thalli cultured on agar (control, 33 µM; 30×, 1 mM; 200×, 6.5 mM $MnCl_2$). **B)** Microscopy images of thalli cultured on agar (a, Control; b, 30×; c, 200×). **C)** Epifluorescence microscopy images of chloroplast surfaces of thalli (d, Control; e, 30×; f, 200×). Mn deficiency: **D)** Metal content of intact chloroplasts isolated from thalli cultured on starch (Starch + Mn, 33 µM Mn; Starch − Mn, without Mn). **E)** Microscopy images of chloroplasts in thalli (g, Starch + Mn; h, Starch − Mn). **F)** Epifluorescence microscopy images of chloroplast surfaces of thalli (i, Starch + Mn; j, Starch − Mn). Scale bars in B and E represent 200 µm; scale bars in C and F represent 10 µm. Error bars in A and D represent standard errors. Stars in A and D indicate significant differences, compared to the control condition, based on a Mann–Whitney test (***$P < 0.001$; $N \geq 3$ biological replicates).

whole thalli. We observed an increase from 2 to 175 µg Mn mg Chl^{-1} in the 200× condition compared to the Control. We determined the total chlorophyll content of the thalli to determine the proportion of Mn allocated to chloroplasts (Figures 1B and 2A; Supplemental Table S1). About 7% to 13% of the total Mn content of the thalli was detected inside the isolated chloroplasts with 13% in Control and 30× and 7% in 200×. There were no significant changes in the chloroplast Fe and Mg concentrations under Mn excess.

We used first bright-field and epifluorescence microscopy to see whether Mn excess changes the morphology of the cells as well as the number of chloroplasts (Figure 2B). In Control Agar, most chloroplasts show typical plant-type spherical morphology, while in 30×, there was a divergence from this typical architecture. Some chloroplasts had a deformed shape. In 200×, this progression of deformation of the morphology was further enhanced and the chloroplasts were smaller on average (Figure 2C, Supplemental Figure S2). Next, we used

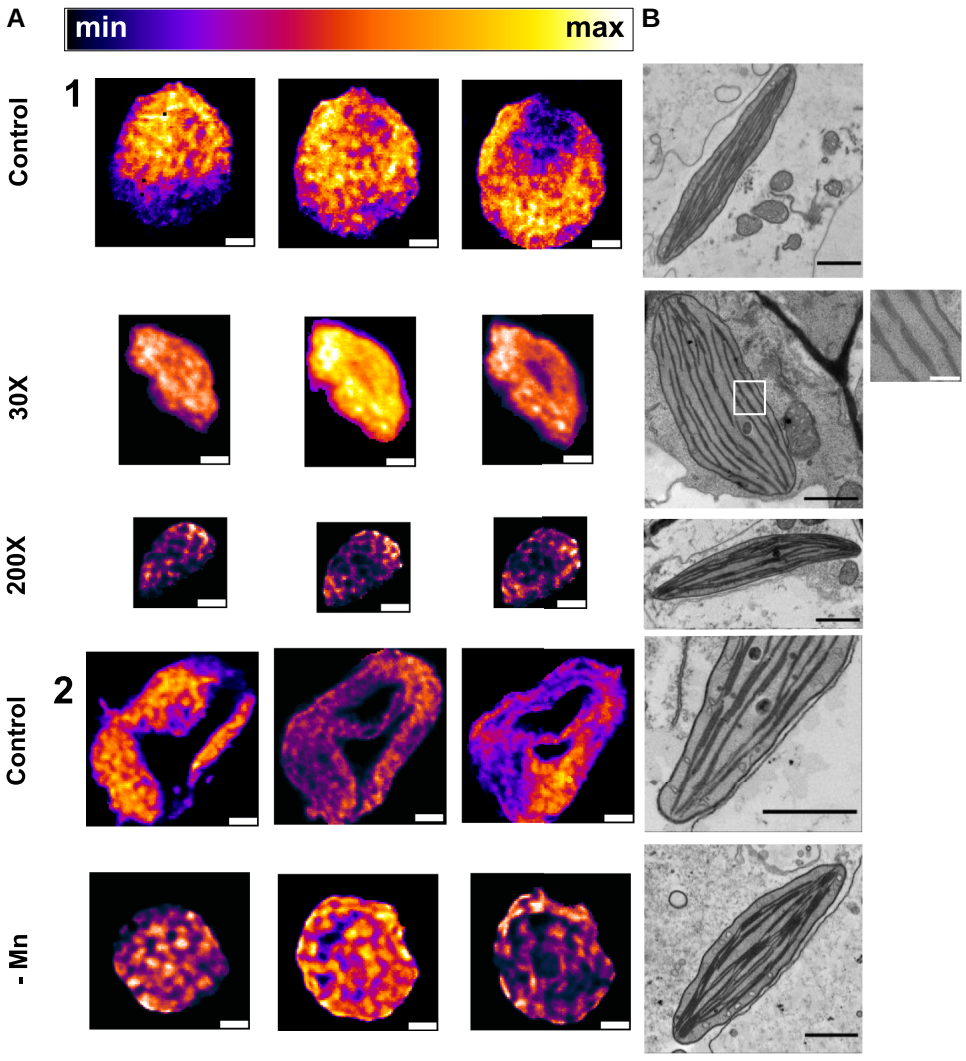

Figure 3. Organization of chloroplast membranes as evidenced by room temperature in vivo super-resolution chlorophyll fluorescence emission nanoscopy and by TEM. **A)** Super-resolution fluorescence microscopy. 1) Agar Control, 30× and 200× conditions and 2) Starch Control and Starch − Mn. For each culture condition, reading from left to right, the 3 reconstructed fluorescence maps are separated by 300 nm in the axial (z) direction. The false-color scale is represented by horizontal color bar (minimum, black; maximum, white). Scale bar: 1 µm. One chloroplast is represented by a total of 10 chloroplasts analyzed for each condition. **B)** TEM images. 10–20 chloroplasts were analyzed, exhibiting the same features for each culture condition. Scale bar: 1 µm (except for the digitally enhanced insert, 200 nm).

super-resolution fluorescence nanoscopy and transmission electron microscopy (TEM) to determine better the change in the organization of the thylakoid membranes triggered by excess Mn (Figure 3). At physiological temperatures, chlorophyll fluorescence is mainly due to PSII emission, which is essentially concentrated in the grana lamellae (for reviews, see Dekker and Boekema 2005; Kirchhoff 2019). Hence, the fluorescence images partly represent the spatial organization and relative abundance of grana stacks in in vivo chloroplasts. The organization of the chloroplast in the Control (Figure 3A top panel) is similar to that of *Arabidopsis thaliana* (Iwai et al. 2018; Streckaite 2021) with a "round" shape and the presence of numerous grana stacks visualized as highly fluorescent yellow/orange patches in the false-color images, albeit with a less clear separation between stroma and grana lamellae. Under the 30× condition, the chloroplast is smaller, indicating a more compact spatial organization of the interconnected granae. Furthermore, the presence of a non-fluorescent region was observed in the center corresponding to a void in bright-field images. In 200×, the smaller chloroplasts still exhibited strong chlorophyll fluorescence emissions with a well-developed distribution of patches indicative of thylakoid grana stacks. Electron microscopy images confirm clear grana stacking under control and 200× conditions, while the organization at 30× was different with 3 thylakoid membranes always attached to each other concomitant with a lack of major grana stack formation (Figure 3B, TEM insert). This uniform distribution of attached membranes under

Table 3. Chl *a*/*b* ratio and electron transport capacities of thylakoids from thalli cultured on manganese excess and deficiency

Parameter	Experimental condition				
	Ctrl	30×	200×	Starch + Mn	Starch − Mn
Chl *a*/*b*	1.23 ± 0.09	1.30 ± 0.10	0.97 ± 0.06	0.95 ± 0.22	0.91 ± 0.20
F_v/F_m	0.775 ± 0.005	0.773 ± 0.003	0.765 ± 0.004	0.772 ± 0.012	0.751* ± 0.004
PSI/PSII	1.47 ± 0.02	1.42 ± 0.01	1.19* ± 0.02	1.11 ± 0.02	1.51* ± 0.01
PSII activity	48 ± 13	43 ± 17	15.0*** ± 5.1	30 ± 9	22 ± 8
PSI activity	116 ± 20	114 ± 27	100 ± 40	59 ± 8	75* ± 16

Chlorophyll content was determined after extraction in acetone. PSI to PSII ratio was determined by integrating the area of the fluorescence at 77 K ($\lambda_{max725}/\lambda_{max685}$). PSII and PSI activities (μmol O_2 μg chl^{-1} h^{-1}) were measured using an O_2 electrode. PSII activity was measured as oxygen evolution in the presence of 1 mM 2,6-dichloro-1,4-benzoquinone (DCBQ), 10 mM NH_4Cl. PSI activity was measured as oxygen uptake in the presence of 10 μM DCMU, 5 mM ascorbate, 30 μM DCPIP, 500 μM methylviologen, and 10 mM NH_4Cl. Mean value and SE are given. Stars indicate significant difference compared to the control condition, based on a Mann–Whitney test (*$P < 0.01$, ***$P < 0.001$, $N = 6$).

30× Mn is in agreement with the quasi-uniform false-color chlorophyll emission maps observed using in vivo fluorescence nanoscopy, attributed to mainly PSII emission.

Since the size of the chloroplasts and the distribution of the chlorophyll fluorescence within the chloroplasts were affected by the growth conditions, photosynthesis was studied in more detail. Table 3 presents that the Chl *a*/*b* ratio remained unchanged at 30× but decreased at 200× Mn, indicating that the antenna size relative to the reaction center increased since Chl *b* is a major constituent of the light-harvesting complex II (LHCII). The 77 K fluorescence emission spectra (Figure 4A) showed 3 characteristic peaks at 685, 695, and 725 nm; the former 2 peaks are attributed to LHCII and PSII, and the latter to PSI with its antenna (Satoh and Butler 1978). For chloroplasts isolated from thalli grown at 200×, the emission attributed to PSI decreased relative to that of PSII, while there was no change when grown at 30× (Figure 4A). In line with the lower PSI fluorescence relative to PSII fluorescence in 200×, the capacity of PSI electron transport was slightly lower although the effect was not statistically significant (Table 3). However, the capacity of PSII electron transfer was significantly decreased. A damaging effect of high Mn concentration on PSII activity was confirmed by fluorescence induction curves (Figure 4B). The appearance of the K-phase under 200× condition can be attributed to the damage to the Mn_4CaO_5 cluster at the PSII donor side according to Strasser (1997). In 200×, maximum quantum yield of PSII (F_v/F_m) and chlorophyll quenching fluorescence were altered during illumination with actinic light, but there was no increase in the susceptibility of PSII to photoinhibition (Table 3, Supplemental Figures S3 and S4).

Part II: Mn deficiency affects the photosynthetic apparatus and may favor cyclic electron flow

In the following, we investigated the effect of Mn starvation on *M. polymorpha*. Agar plates were not suitable to induce Mn deficiency since agar contains too much Mn as an impurity (12.8 ± 0.4 μM). Therefore, we substituted agar with starch as a gelling agent. Gemmae were cultured for 2 wk on Gamborg's B5 Agar medium (33 μM $MnCl_2$) before young thalli were transferred to Mn-free Gamborg's B5 Starch medium with or without the addition of Mn (33 μM Mn). It was not possible to culture gemmae directly on starch because they were not able to develop. Figure 1C shows that plants exhibited no visible growth defect after 1 week culturing on Starch Control or without Mn. However, chlorophyll fluorescence showed a clear decrease in the quantum yield of PSII (F_v/F_m) was lower when no $MgCl_2$ had been added to the medium (Supplemental Figure S5). The amount of metals in thalli was measured (Figure 1D). The use of starch allowed a reduction of Mn content from 75 μg Mn g DW^{-1} (Starch Control) to 20 μg Mn g DW^{-1} (Starch − Mn). Fe and Mg contents were not affected.

As for Mn excess, a metabolic analysis was carried out. No significant difference in the metabolomics profiles was observed between the 2 starch conditions (Supplemental Table S1), while there were clear differences between Agar Control and Starch Control (Supplemental Table S2). The activity measurements of the antioxidant enzymes showed a significant decrease in the activity of type III peroxidases (Table 2). Using a spin-trapping assay, the generation of $^{\bullet}OH$ derived from $H_2O_2/O_2^{\bullet-}$ was detected in starch-grown plants. ROS levels were 2 times higher in the Starch − Mn condition.

Next, the impact of Mn deficiency on chloroplasts was investigated. The measurements (Figure 2D) revealed a decrease in the Mn content by about 50% in the Starch − Mn condition compared with the Starch Control. There was a tendency that the Starch − Mn growth condition lowers slightly the Fe and Mg content; however, the differences were not statistically significant. Overall, the metal content (Mn, Fe, and Mg) of the chloroplasts under starch conditions was almost double compared to chloroplasts from thalli grown under Agar Control conditions. This may be due to effects on the metal uptake and transport system or also be connected to a higher intactness of the isolated chloroplasts. The epifluorescence microscopy images (Figure 2F) showed more "horseshoe-shaped" chloroplasts under the Starch Control condition. In Starch − Mn, chloroplasts appeared rounder. These observations were confirmed by super-resolution nanoscopy (Figure 3B); however, the area of the chloroplasts was unaltered (Supplemental Figure S2). In the Starch Control, the thylakoid membranes were organized in grana/lamellae-like structures. In the Starch − Mn condition, the chloroplasts had fewer voids in the 3D volume.

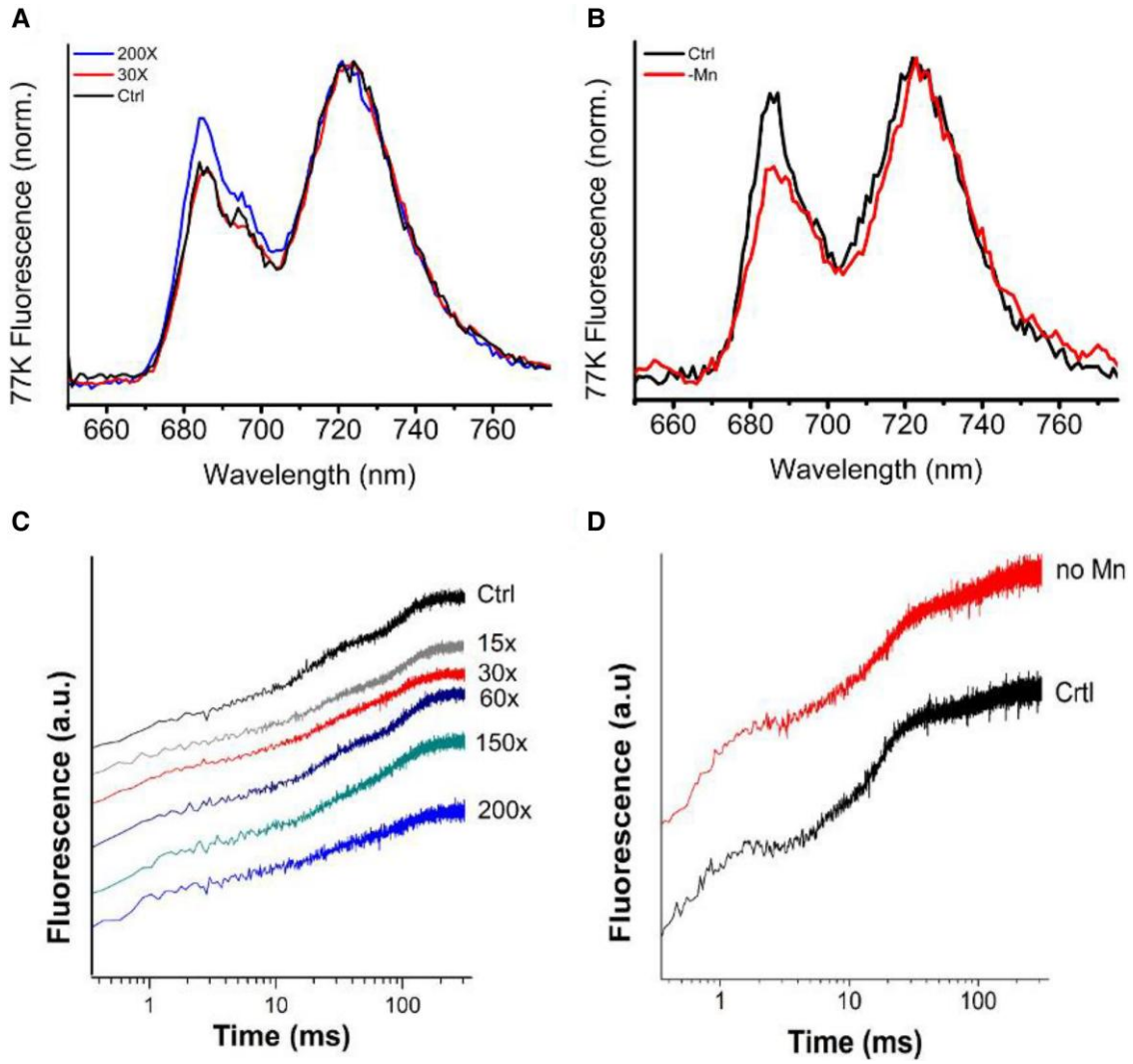

Figure 4. Chlorophyll fluorescence at 77 K and room temperature. **A)** 77 K fluorescence emission of chloroplasts extracted from thalli grown on agar: Ctrl (black), 30× (red), and 200× (blue, upper trace at 685 nm) ($N = 3$, biological replicates). **B)** Same as (a) carried out on starch-cultivated thalli with (Ctrl, black) or without $MnCl_2$ (−Mn, red, upper trace at 685 nm). Spectra in A and B were normalized to the maximum emission at 725 nm. **C)** Room-temperature fluorescence induction curves (OJIP) were measured on 5-min dark-adapted thalli by the application of a saturating flash with 300 ms duration. Culture conditions as in A. **D)** Fluorescence induction curves on thalli grown as in B. One representative curve is shown for each condition.

Compared with a standard chloroplast as represented in the Agar Control (Figure 3A, top panel), or Arabidopsis (Iwai et al. 2018; Streckaite 2021), the strongly fluorescent regions were localized more distinctly, indicating a change in the mesoscopic organization of the thylakoid membrane. This indicates smaller grana stacks with a more pronounced segregation between them and the stroma lamellae as confirmed by TEM. The TEM image shows a much higher degree of stacking of the thylakoid membranes (Figure 3B).

The 77 K fluorescence (Figure 4B) showed a decrease in the emission at 680 nm in chloroplasts isolated from Starch – Mn thalli, indicating a loss of PSII content compared with PSI. PSII activity was lower (Table 3). The quantum yield of PSII, F_v/F_m, was significantly lower upon Mn deficiency. PSI activity increased significantly, confirming the change in the PSI/PSII ratio under Mn deficiency seen in 77 K fluorescence spectra. In the Starch – Mn condition, the fluorescence induction curves showed a dip phase at about 2 ms, indicative of damage to the Mn_4CaO_5 cluster at the PSII donor side (Figure 4D).

Figure 5 shows changes in room temperature chlorophyll fluorescence upon illumination with actinic light. Upon Mn deficiency, energy dissipation as the heat was enhanced (qN; Figure 5C). However, photochemical quenching (qP; Figure 5D) was not affected. Furthermore, the slightly higher minimum fluorescence level during the recovery phase (post-illumination fluorescence transient, PIFT) upon Mn deficiency indicates an increase in chlororespiratory and/or cyclic electron flow. To show whether the stability of PSII or the repair of damaged PSII was affected under Mn deficiency, photoinhibition experiments were carried out with or without the protein synthesis inhibitor lincomycin

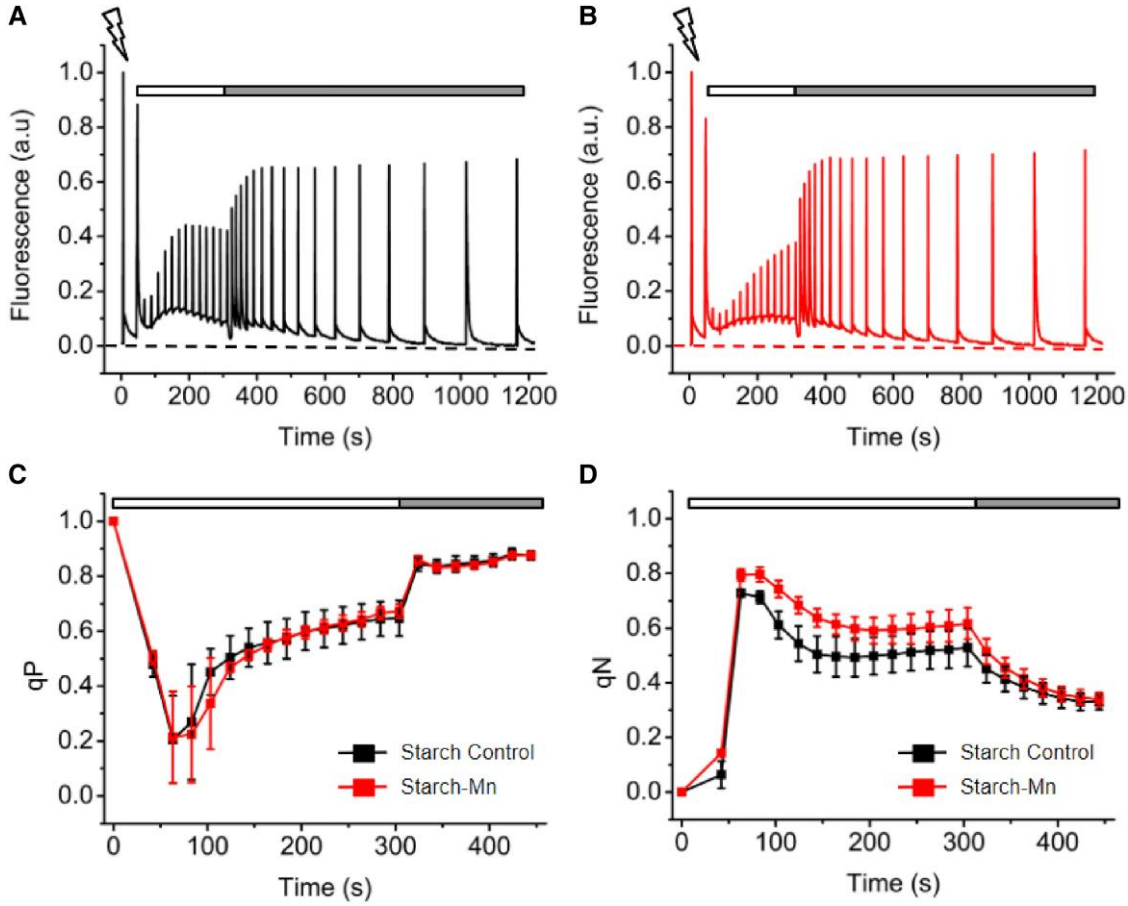

Figure 5. Analysis of variable chlorophyll fluorescence in Mn deficiency. **A)** and **B)** Induction and recovery fluorescence curves were measured on thalli transferred for 1 week to starch medium with (black) or without added $MnCl_2$ (red). After 5 min dark adaptation, thalli were exposed to a measuring light to determine the minimum fluorescence level (dashed lines) and to a saturating flash to obtain the maximum fluorescence level. Actinic light (50 µmol photons m^{-2} s^{-1}) was applied for 5 min (white bar). Recovery in the dark was followed (gray bar). **C)** qN and **D)** qP parameters were calculated, thanks to saturating flashes applied during the light and dark period. Mean values and standard deviation are given in **C** and **D** ($N = 12$, 3 biological replicates). C: lower trace, without added $MnCl_2$; D: upper trace, without added $MnCl_2$.

(Figure 6). Plants cultivated on Starch – Mn were more susceptible to high light in the absence of lincomycin. In the presence of lincomycin, the opposite was observed with PSII in plants cultivated on Starch – Mn being more resistant to the photoinhibitory treatment. This may be explained by the higher nonphotochemical quenching (NPQ) protecting the photosynthetic apparatus. A higher NPQ was observed also in the presence of lincomycin (Supplemental Figure S6).

The higher PSI fluorescence at 77 K, the higher NPQ, and the protection of PSII against photoinhibition in plants cultivated on Starch – Mn may indicate that cyclic electron transport is favored under these conditions. Absorption changes of P700 show that P700 is more slowly oxidized, both in red actinic and in far-red light, in plants cultivated on Starch – Mn indicating that more electrons are available in the electron transport chain (Figure 7A). To show that indeed more electrons are available for $P700^+$ reduction at the luminal side, we determined the yield of donor-side limitation, Y(ND) as a function of the intensity of the actinic light. Figure 7B shows the less donor-side limitation of PSI over a wide range of light intensities in plants cultivated on Starch – Mn compared to those cultivated on Starch Control. These data further indicate a higher activity of cyclic electron flow under Mn deficiency. Under both conditions, acceptor side limitation at the stromal side of PSI was not observed because Marchantia possesses flavodiiron proteins that use ferredoxin as an electron donor to reduce oxygen to water (Shimakawa et al. 2021).

Discussion

In this study, we established growth conditions for manganese excess and deficiency in *M. polymorpha*. Marchantia can absorb up to 25 mg Mn g DW^{-1} (Figure 1B) which is higher than the hyperaccumulator *Polygonum lapathifolium* that contains approximately 18 mg Mn g DW^{-1} in its aerial parts (Liu et al. 2016). However, Marchantia shows symptoms of toxicity under the 200× conditions, and thalli

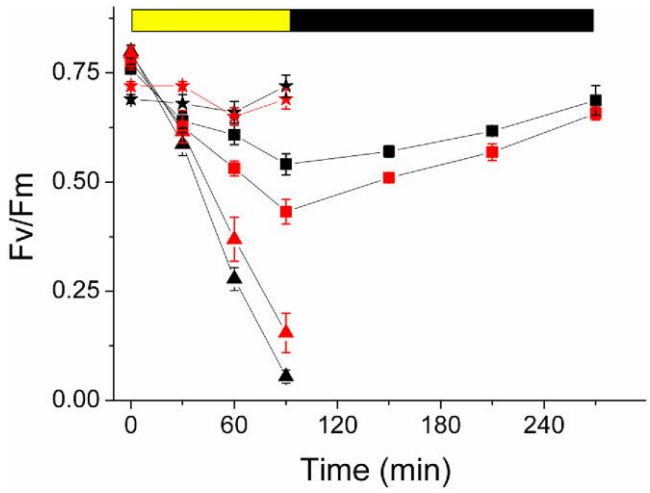

Figure 6. Photoinhibition in Mn deficiency in the absence and presence of lincomycin. Photoinhibition was measured on starch-cultivated thalli with (black symbols) or without $MnCl_2$ (red symbols). F_v/F_m was followed during exposure to high light (800 µmol photons $m^{-2}s^{-1}$) for 90 min (yellow bar) and during the recovery at room light (black bar). Squares: without lincomycin; lower trace without $MnCl_2$, triangles: with lincomycin; upper trace without $MnCl_2$ As a control, lincomycin samples incubated in the dark are shown (stars). Mean values and standard errors are given ($N = 6$, 2 biological replicates).

only survive for a few weeks. Therefore, Marchantia does not qualify as a hyperaccumulator despite its high Mn uptake capacity. Mn excess conditions induced an increase in SOD and peroxidase (PRX) activity, while catalase activity decreased (Table 2). An increase in SOD activity could reflect a higher amount of MnSOD present under Mn excess conditions. The metabolomics analysis showed that known stress-induced metabolites accumulate upon excess Mn (Table 1; Supplemental Figure S2 and Tables S2 and S3); however, the metabolomics response of Marchantia is distinct from that of angiosperms and requires in-depth functional analysis of metabolites and metabolic pathways. An excess of Mn affected the ratio between it and other metals (e.g. Fe and Mg) in both thalli and chloroplasts. Indeed, cation transporters are known not to be completely selective under stressed conditions (Vert et al. 2002; Ducic et al. 2005; Lei et al. 2007; Millaleo et al. 2010; Barberon et al. 2011); well-documented examples of excess of Mn in the soil are known to perturb the absorption and translocation of other elements, including iron, magnesium, and phosphorus (Ducic et al. 2005; Lei et al. 2007; Millaleo et al. 2010), causing Fe deficiency in plants. However, Marchantia grown at 200 × does not show alterations in the Fe and Mg content inside the thalli (Figures 1B and 2A). Nevertheless, an alteration in the Mn/Fe ratio may induce Fe deficiency through competitive binding. Fe deficiency is known to affect primarily PSI that is rich in 4Fe4S clusters. As shown in Figure 4B, PSI content is lowered in comparison to PSII in 200×. A similar reduction of PSI upon exposure to Mn excess has been reported for Arabidopsis (Millaleo et al. 2013). Aside PSI, the water-splitting activity of PSII seems also to be affected in the 200 × condition as seen by the appearance of the K-phase in fluorescence induction curves (Figure 4C) and the decrease in PSII activity (Table 2). A toxic effect of Mn excess on PSII activity is in accordance with data on angiosperms (Liang et al. 2019); 200 × Mn not only negatively affected the photosynthetic apparatus but also led to a reduction in chloroplast size and an alteration of the well-separated grana stack and stroma lamellae distribution (Figures 2 and 3).

Transfer of thalli from agar to starch plates allowed to establish Mn deficiency conditions. Growth in starch allowed lowering the Mn content drastically in the thalli to 21 µg Mn g DW^{-1}. According to Mengel and Kirkby (1987), the minimum Mn content required for the growth of angiosperms is about 20 to 40 mg Mn kg DW^{-1}, and most angiosperms usually contain 30 to 500 mg Mn kg DW^{-1}. Manganese deficiency led to a decrease in F_v/F_m, a change in the ratio of the activity PSI/PSII (Table 3), and less PSII content relative to PSI according to 77 K fluorescence (Figure 4B). In angiosperms, Mn deficiency lowers PSII activity while PSI activity remains unaffected (Homann 1967; for review see Schmidt et al. 2016). Furthermore, the structural organization of the thylakoids was affected (Figure 3). It is known that Mn deficiency leads to disorganization of the thylakoid membrane in angiosperms (Mercer et al. 1962; Homann 1967). In *M. polymorpha*, the smaller compartmentation of the grana stacks could be partly responsible for the changes in electron transport. In addition to a change in the stoichiometry between active PSI and active PSII, a different distribution of photosynthetic complexes may favor cyclic electron flow around PSI by allowing the formation of supercomplexes likely to be required for cyclic electron flow (Iwai et al. 2010). As shown in Figure 7, thalli grown on Starch – Mn show less limitation of electron donation to $P700^+$ than those of the Starch Control indicating a stimulation of cyclic electron flow under Mn deprivation. Cyclic electron flow is known to be induced under specific physiological conditions like anaerobiosis in *Chlamydomonas reinhardtii* (Joliot et al. 2022). Changes in the organization of PSI complexes were also observed under Mn limitation in cyanobacteria (Salomon and Keren 2011). Increased cyclic electron flow generates a higher proton gradient across the thylakoid membrane and thereby an increase in NPQ (Figure 5C). A higher NPQ protects PSII against photoinhibition as seen when thalli grown on Starch – Mn were exposed to high light in the presence of lincomycin (Figure 6), while they were more susceptible to photoinhibition in the absence of lincomycin (Figure 6) likely due to a slowdown of PSII repair. A slowdown of PSII repair under Mn deficiency has been observed previously in the Mn transporter mutant *nramp3nramp4* in Arabidopsis (Lanquar et al. 2010). The repair of PSII may be slowed down in the light because of the higher ROS levels in Starch – Mn (Table 2) that affects the synthesis of the D1 protein (Nishiyama et al. 2011).

In conclusion, we show here that unfavorable Mn concentrations during the growth of Marchantia affect not only the

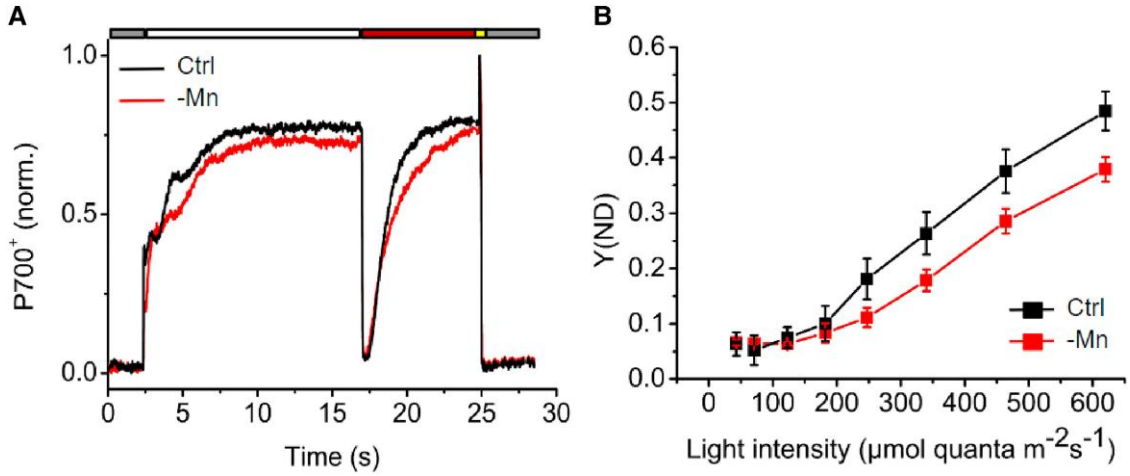

Figure 7. Activity of PSI in Mn deficiency. **A)** Normalized $P700^+$ signal was obtained on thalli cultivated on Starch (+Mn, black, upper trace; −Mn, red, lower trace). The redox state of the PSI primary donor P700 was monitored through the changes in absorbance at 830 versus 875 nm. Leaves were kept in the dark for 5 min prior to the measurements. Thalli were exposed to actinic light for 15 s (white bar) and to far-red light until reaching a plateau (red bar). Then, a saturating flash was applied (yellow bar) and the decay was observed in the dark (gray bar). **B)** PSI donor-side limitation Y(ND) based on saturating pulse analyses. Following the initial determination of maximal oxidation of P700, actinic light of the indicated intensities was given for 180 s. Mean values and standard deviation are given ($N = 6$, 2 biological replicates).

photosynthetic apparatus but also the organization of the thylakoid membrane. Future work is needed to explore the link between changes in the organization and stacking of the thylakoid membrane and stimulation of cyclic electron flow under Mn deficiency.

Materials and methods

Plant growth conditions

Gemmae from *M. polymorpha*, Takaragaike (Tak-1) accession (male) were asexually cultured on ½ Gamborg's GB5 1% (w/v) Agar medium (Gamborg et al. 1968) for 2 weeks under a light–dark cycle of 16-h light, 22°C, 120 µmol quanta $m^{-2}s^{-1}$, white fluorescent lamp/8 h dark, 20°C. For Mn excess condition, young thalli were transferred to ½ Gamborg's GB5 1% Agar medium containing 33 µM (control), 0.5 mM (15×), 1 mM (30×), 2 mM (60×), 5 mM (150×), or 6.5 mM (200×) $MnCl_2$ for 1 week before measurements. According to the metal quantification, the control medium contained 2.52 ± 0.27 µg Mn g^{-1} fresh weight of the solid medium. For Mn deficiency, young thalli were transferred on ½ Gamborg's GB5 6% starch (w/v) medium with or without the addition of 33 µM $MnCl_2$ for 1 week before performing measurements. According to the metal quantification, the starch medium with $MnCl_2$ contained 2.03 ± 0.13 µg Mn g^{-1}, and the medium without the addition of $MnCl_2$ contained 0.26 ± 0.08 µg Mn g^{-1} fresh weight of the solid medium.

Chloroplast and thylakoid isolation

About 10 g of thalli was collected, the media carefully mechanically removed, and grounded in 100 ml of GR buffer (50 mM Hepes-KOH pH 7.5, 0.33 M sorbitol, 1 mM $MgCl_2$, 2 mM EDTA, 5 mM Na-ascorbate) with a spatula of BSA. The slurry was filtered through 2 layers of Miracloth and centrifuged at 1,200 × *g* (4°C) for 7 min. Pellets were resuspended in 2 m of GR buffer and then layered on the top of a Percoll gradient [15 ml of 30% Percoll/GR buffer (v/v) and 10 ml of 70% Percoll/GR buffer v/v], centrifuged at 7,000 × *g* (4°C) for 17 min (no brake). Intact chloroplasts were collected and washed in 25 ml of GR buffer; centrifugation 1,500 × *g* (4°C) for 5 min. The intactness was checked by light microscopy. For thylakoids, the same procedure was used without the percoll gradient.

Metal quantification

Thalli were collected and dried at 70°C for 2 days before being weighed. About 1 ml of nitric acid (65%) was added to 1 mg of plant material. For intact chloroplasts, the chlorophyll concentration was adjusted to 100 µg chl ml^{-1} before the addition of 2.5 volume of nitric acid. After 10-fold dilution in trace-metal-free water, the metal content of the samples was determined by atomic emission spectroscopy using an MP AES 1200 spectrometer (Agilent, USA).

Super-resolution microscopy

For each sample, a small quantity of thallus was placed in a sandwich of 2 glass coverslips (22 mm diameter, Paul Marienfeld GmbH & Co. KG), sealed, and placed inside an in-house built sample holder. The sample holder was fixed to a nano-positioning system (P-733.2CD, P-725.4CD, E-725.3CD, Physikinstrumente) coupled to an inverted microscope (Ti-U, Nikon) equipped with a CFI Apochromat Lambda 100× oil immersion objective. Room-temperature fluorescence emission was recorded by an iXon ULTRA 897 camera in conventional mode, gain 3 (Andor Technology Ltd.,

Belfast), coupled to the microscope with a custom-made Optomask (Cairn Research Ltd, Faversham). The total chlorophyll fluorescence emission was isolated using a dichroic mirror/emission filter doublet (59022BS/ET655LP, Chroma Technology Corporation). Epifluorescence images were recorded using an excitation provided by a plasma light source (HPLS245 Thorlabs Inc.) and an excitation filter (MF469-35 Thorlabs Inc.). The excitation source for the laser-scanning measurements was a 445-nm emitting laser (OBIS LX, Coherent Inc.) at 100 nW intensity at the sample. Laser scanning and final image reconstruction [resolution (d) $d_{xy} = 126$ nm, $d_z = 320$ nm] were as previously described (Streckaite 2021) with a dwell time of 10 to 30 ms, 60-nm X/Y-scan steps, and 300-nm Z-scan steps.

Transmission electron microscopy

About 1-mm strips of thalli were cut under glutaraldehyde/paraformaldehyde fixative and impregnated by the 1% osmium (w/v) and 1.5% potassium hexacyanoferrate (w/v) en bloc staining protocol as described (Hawes et al. 1981; Juniper et al. 1982); 70-nm-thick sections were cut with an EM UC6 ultramicrotome (Leica Microsystems) and deposited on to copper grids. Ultrathin sections were stained with 2% uranyl acetate (w/v) (Merck) and Reynolds lead citrate according to standard procedures. Grids were examined under a JEOL 1400 TEM operating at 80 kV (JEOL, http://www.jeol.com). Images were acquired using a 9-megapixel high-speed camera (RIO9; Gatan, http://www.gatan.com) and processed using Digital Micrograph (Gatan).

Pigment analysis

Thalli were weighed and incubated in 100% acetone for 16 h in the dark. For complete pigment extraction, acetone incubation was repeated 3 times. The pigment extract was diluted to 80% acetone (v/v) before measurement. Chlorophyll *a* and chlorophyll *b* contents were calculated according to Porra and Scheer (2019).

77K Chlorophyll fluorescence measurements

Fluorescence spectra of intact chloroplasts diluted in GR buffer were measured with a Carry Eclipse fluorimeter (Agilent, USA); excitation wavelength: 430 nm. The spectra were normalized to the intensity of the PSI emission.

Chlorophyll fluorescence analysis at room temperature

Chlorophyll fluorescence analysis was performed on 5 min dark-adapted thalli using a Dual-PAM-100 fluorimeter (Walz, Effeltrich, Germany). F_m and F_m' were determined using saturating flashes (10,000 µmol quanta $m^{-2}s^{-1}$, duration 300 ms). F_o, minimum and F_m, maximum fluorescence in a dark-adapted sample; F_m', maximum fluorescence and F', fluorescence emission from a light-adapted sample. Induction and recovery curves were measured using actinic light of 50 µmol quanta $m^{-2}s^{-1}$: $F_v/F_m = (F_m - F_0)/F_m$, $qN = (F_m - F_m')/(F_m - F_0')$, and $qP = (F_m' - F)/(F_m' - F_0')$. For induction curves (OJIP), one saturating flash was given.

Photoinhibition

Thalli were placed on wet filter paper and illuminated with white light (800 µmol quanta $m^{-2}s^{-1}$) LED panel SL3500 (Photon Systems Instrument, Drasov, Czech Republic). For recovery, samples were placed in low light (10 µmol quanta $m^{-2}s^{-1}$). When indicated, thalli were incubated in lincomycin (1 g L^{-1}) for 4 h prior to the photoinhibition treatment. F_v/F_m was measured using an Imaging-PAM (Walz, Effeltrich, Germany).

P700 measurements

P700 absorbance was measured using a Dual-PAM-100 fluorometer (Walz, Effeltrich, Germany). Near-infrared measuring lights (830 and 870 nm) were applied to measure the transmittance of oxidized P700. Prior to the measurements, the plants were kept in the light in the growth chamber so that the Calvin–Benson cycle enzymes were active. Five minutes dark-adapted thalli were exposed to actinic light followed by far-red light. Then, a saturating flash was given at the end of the far-red light period. To determine quantum yields of PSI donor, Y(ND), and acceptor side limitations, Y(NA), saturating pulse analysis was used (Klughammer and Schreiber 1994). Each actinic light intensity was applied for 180 s before determining Y(ND) and Y(NA).

Antioxidant enzymes activity

Thalli were harvested and ground in 50-mM HEPES buffer pH 6.5. The slurry was filtered through one layer of Miracloth, centrifuged for 5 min at 10.000 × g (4°C). Protein concentration in the crude extract was determined by amido black since the supernatant contained pigments (Schaffner and Weissmann 1973). About 10 µg ml^{-1} protein was used for the enzymatic tests. Guaiacol peroxidase activity was determined spectrophotometrically by measuring the oxidation of guaiacol to tetraguaiacol at 470 nm (ϵ: 26.6 $mM^{-1}cm^{-1}$) (Chance and Maehly 1955). The reaction mixture contained 50 mM NaH_2PO_4/Na_2HPO_4 pH 7.5, 3 mM H_2O_2, and 0.01% (v/v) guaiacol. Catalase activity was measured polarographically at 20°C with a Clark-type electrode in 50 mM Tris buffer pH 8.5 and 1 mM H_2O_2 as substrate. SOD activity was measured using a solution of 500 µM Xanthine, 20 mM HEPES buffer pH 7, 0.2 U ml^{-1} xanthine oxidase, and 100 µM XTT (Na,3′-(1-(phenylaminocarbonyl)-3,4-tetrazolium)-bis-(4-methoxy-6-nitro) benzene sulfonic acid hydrate) as substrate. The kinetics of superoxide production were measured as increase in absorbance at 470 nm, and the SOD activity was determined by following the inhibition of the superoxide production after the addition of the crude extract (Molins et al. 2013). For $^{\bullet}OH$ detection, 15 mg thalli were incubated for 1 h in 3 ml 10 mM phosphate buffer, pH 6.0, 50 mM *N*-tert-butyl-α-(4-pyridyl)nitrone *N*′-oxide (4-POBN), and 4% ethanol (v/v) (Heyno et al. 2008).

Metabolite analysis

GC-MS profiling of metabolites was performed on thalli cultured on Agar Control, 30× and 200× conditions and thalli grown on Starch Control and Starch − Mn. Dried and grounded samples (5 mg of dry weight) were incubated in 1 ml of H_2O/ACN/isopropanol (2/3/3) with 4 mg l^{-1} of ribitol for 10 min at 4°C with shaking at 250 *g* in an Eppendorf Thermomixer. Insoluble material was removed by centrifugation at 20,400 × *g* for 10 min; 700 µl of supernatant was recovered, and 70 µl of a mix of H_2O/MeOH/isopropanol (2/5/2) with 0.3 g L^{-1} of myristic acid d27 was added as an internal standard for retention time locking. Aliquots of each extract (100 µl) extracts were dried for 4 h at 30°C in a Speed-Vac and stored at −80°C. After thawing, samples were dried again in a Speed-Vac for 1 h at 30°C before adding 10 µl of 20 mg ml^{-1} methoxyamine in pyridine to the samples. The reaction was performed for 90 min at 30°C under continuous shaking in an Eppendorf thermomixer. A volume of 90 µl of *N*-methyl-*N*-trimethylsilyl-trifluoroacetamide was then added and the reaction continued for 30 min at 37°C. After cooling, 80 µl were transferred to an Agilent vial for injection. Four hours after derivatization, 1 µl sample was injected in splitless mode on an Agilent 7890B gas chromatograph coupled to an Agilent 5977A mass spectrometer (column: RESTEK RXI 5SIL MS 30MX0.25MMX0.25UM). An injection in split mode with a ratio of 1:30 was systematically performed for the quantification of saturated compounds. Raw Agilent data files were analyzed with AMDIS https://chemdata.nist.gov/dokuwiki/doku.php?id=chemdata:amdis. The Agilent Fiehn GC-MS Metabolomics RTL Library was employed for metabolite identifications. Peak areas were determined with the Masshunter Quantitative Analysis (Agilent) in splitless and split 30 modes. Peak areas were normalized to ribitol and dry weight. Metabolite contents are expressed in arbitrary units (semi-quantitative determination).

Acknowledgments

We thank Claire Boulogne (I2BC) for performing electron microscopy.

Author contributions

M.M. and A.K.-L. designed the project. M.M., U.H., T.H., F.G., B.G., A.G., S.T., and A.K.-L. performed the experiments and analyzed the data. M.M. and A.K.-L. wrote the initial version of the manuscript that was read and revised by all authors.

Supplemental data

The following materials are available in the online version of this article.

Supplemental Table S1. Chlorophyll and Mn content in thalli grown in Mn excess.

Supplemental Table S2. List of 96 metabolites identified by GC-MS in *M. polymorpha*.

Supplemental Table S3. Metabolites significantly decreased in starch condition compared with agar control in *M. polymorpha*.

Supplemental Figure S1. Metabolite analysis in *M. polymorpha* grown in Mn excess condition.

Supplemental Figure S2. Estimation of the chloroplast size under the different growth conditions.

Supplemental Figure S3. Chlorophyll fluorescence at room temperature in *M. polymorpha* grown in control and Mn excess conditions.

Supplemental Figure S4. Photoinhibition of photosystem II in *M. polymorpha* grown in control and Mn excess condition in the presence and absence of lincomycin.

Supplemental Figure S5. Chlorophyll fluorescence (F_v/F_m) in *M. polymorpha* grown on starch plates in low Mn concentrations.

Supplemental Figure S6. qN determination in the presence of lincomycin in *M. polymorpha* grown on starch in control and Mn-deficient conditions.

Funding

This work was supported by the Labex Saclay Plant Sciences-SPS (ANR-17-EUR-0007), the platform of Biophysics of the I2BC supported by the French Infrastructure for Integrated Structural Biology (FRISBI; grant number ANR-10-INSB-05), and IBiSA and France-BioImaging infrastructure supported by the Agence Nationale de la Recherche (ANR-10-INBS-04, call "'investissements d'Avenir"). M.M. is supported by a CEA PhD fellowship.

Conflict of interest statement. None declared.

Data availability

Data will be made available on demand.

References

Alam S, Akiha F, Kamei S, Huq SMI, Kawai S. Mechanism of potassium alleviation of manganese phytotoxicity in barley. J Plant Nutr. 2005:**28**(5):889–901. https://doi.org/10.1081/PLN-200055572

Alejandro S, Höller S, Meier B, Peiter E. Manganese in plants: from acquisition to subcellular allocation. Front Plant Sci. 2020:**11**: article 300. https://doi.org/10.3389/fpls.2020.00300

Amao Y, Ohashi A. Effect of Mn ion on the visible light induced water oxidation activity of photosynthetic organ grana from spinach. Catal Commun. 2008:**10**(2):217–220. https://doi.org/10.1016/j.catcom.2008.08.022

Barberon M, Zelazny E, Robert S, Conéjéro G, Curie C, Friml J, Vert G. Monoubiquitin-dependent endocytosis of the iron-regulated transporter 1 (IRT1) transporter controls iron uptake in plants. Proc Natl Acad Sci U S A. 2011:**108**(32):E450–E458. https://doi.org/10.1073/pnas.1100659108

Blamey FPC, Hernandez-Soriano M, Cheng M, Tang C, Paterson D, Lombi E, Hong Wang W, Scheckel KG, Kopittke PM. Synchrotron-based techniques shed light on mechanisms of plant sensitivity and tolerance to high manganese in the root environment. Plant Physiol. 2015:**169**(3): 2006–2020. https://doi.org/10.1104/pp.15.00726

Bowler C, Van Camp W, Van Montagu M, Inzé D, Asada K. Superoxide dismutase in plants. CRC Crit Rev Plant Sci. 1994:**13**(3): 199–218. https://doi.org/10.1080/07352689409701914

Chance B, Maehly AC. Assay of catalases and peroxidases. Methods Enzymol. 1955:**2**:764–775. https://doi.org/10.1016/S0076-6879(55)02300-8

Clairmont KB, Hagar WG, Davis EA. Manganese toxicity to chlorophyll synthesis in tobacco callus. Plant Physiol. 1986:**80**(1):291–293. https://doi.org/10.1104/pp.80.1.291

Corpas FJ, Barroso JB, Palma JM, Rodriguez-Ruiz M. Plant peroxisomes: a nitro-oxidative cocktail. Redox Biol. 2017:**11**:535–542. https://doi.org/10.1016/j.redox.2016.12.033

Dekker JP, Boekema EJ. Supramolecular organization of thylakoid membrane proteins in green plants. Biochim Biophys Acta. 2005:**1706**(1–2):12–39. https://doi.org/10.1016/j.bbabio.2004.09.009

Delhaize E, Gruber BD, Pittman JK, White RG, Leung H, Miao Y, Jiang L, Ryan PR, Richardson AE. A role for the AtMTP11 gene of Arabidopsis in manganese transport and tolerance. Plant J. 2007:**51**(2):198–210. https://doi.org/10.1111/j.1365-313X.2007.03138.x

Ducic T, Polle A. Manganese toxicity in two varieties of douglas fir (*Pseudotsuga menziesii* var. *viridis* and *glauca*) seedlings as affected by phosphorus supply. Funct Plant Biol. 2007:**34**(1):31–40. https://doi.org/10.1071/FP06157

Eisenhut M, Hoecker N, Schmidt SB, Basgaran RM, Flachbart S, Jahns P, Eser T, Geimer S, Husted S, Weber APM, et al. The plastid envelope CHLOROPLAST MANGANESE TRANSPORTER1 is essential for manganese homeostasis in Arabidopsis. Mol Plant. 2018:**11**(7): 955–969. https://doi.org/10.1016/j.molp.2018.04.008

Eroglu S, Meier B, von Wiren N, Peiter E. The vacuolar manganese transporter MTP8 determines tolerance to iron deficiency-induced chlorosis in Arabidopsis. Plant Physiol. 2016:**170**(2):1030–1045. https://doi.org/10.1104/pp.15.01194

Führs H, Behrens C, Gallien S, Heintz D, Van Dorsselaer A, Braun HP, Horst WJ. Physiological and proteomic characterization of manganese sensitivity and tolerance in rice (*Oryza sativa*) in comparison with barley (*Hordeum vulgare*). Ann Bot. 2010:**105**(7):1129–1140. https://doi.org/10.1093/aob/mcq046

Gamborg OL, Miller RA, Ojima K. Nutrient requirements of suspension cultures of soybean root cells. Exp Cell Res. 1968:**50**(1): 151–158. https://doi.org/10.1016/0014-4827(68)90403-5

Hasanuzzaman M, Alhaithloul HA, Parvin K, Borhannuddin Bhuyan MHM, Tanveer M, Moshin SM, Nahar K, Soliman MH, Al Mahmud J, Fujita M. Polyamine action under metal/metalloid stress: regulation of biosynthesis, metabolism, and molecular interactions. Int J Mol Sci. 2019:**20**(13):315. https://doi.org/10.3390/ijms20133215

Hawes CR, Juniper BE, Horne JC. Low and high-voltage electron microscopy of mitosis and cytokinesis in maize roots. Planta. 1981:**152**(5):397–407. https://doi.org/10.1007/BF00385355

Heyno E, Klose C, Krieger-Liszkay A. Origin of cadmiuminduced reactive oxygen species production: mitochondrial electron transfer versus plasma membrane NADPH oxidase. New Phytol. 2008:**179**(3): 687–699. https://doi.org/10.1111/j.1469-8137.2008.02512.x

Homann P. Studies on the manganese of the chloroplast. Plant Physiol. 1967:**42**(7):997–1007. https://doi.org/10.1104/pp.42.7.997

Iwai M, Roth MS, Niyogi KK. Subdiffraction-resolution live-cell imaging for visualizing thylakoid membranes. Plant J. 2018:**96**(1): 233–243. https://doi.org/10.1111/tpj.14021

Iwai M, Takizawa K, Tokutsu R, Okamuro A, Takahashi Y, Minagawa J. Isolation of the elusive supercomplex that drives cyclic electron flow in photosynthesis. Nature. 2010:**464**(7292):1210–1213. https://doi.org/10.1038/nature08885

Joliot P, Sellés J, Wollman FA, Verméglio A. High efficient cyclic electron flow and functional supercomplexes in *Chlamydomonas* cells. Biochim Biophys Acta Bioenerg. 2022:**1863**(8):148909. https://doi.org/10.1016/j.bbabio.2022.148909

Juniper BE, Hawes CR, Horne JC. The relationships between the dictyosomes and the forms of endoplasmic-reticulum in plant-cells with different export programs. Bot Gaz. 1982:**143**(2):135–145. https://doi.org/10.1086/337282

Kirchhoff H. Chloroplast ultrastructure in plants. New Phytol. 2019:**223**(2):565–574. https://doi.org/10.1111/nph.15730

Klughammer K, Schreiber U. An improved method, using saturating light pulses for the determination of photosystem I quantum yield via $P700^+$-absorbance changes at 830 nm. Planta. 1994:**192**(2): 261–268. https://doi.org/10.1007/BF01089043

Lane BG. Oxalate, germins, and higher-plant pathogens. IUBMB Life. 2002:**53**(2):67–75. https://doi.org/10.1080/15216540211474

Lanquar V, Ramos MS, Lelièvre F, Barbier-Brygoo H, Krieger-Liszkay A, Krämer U, Thomine S. Export of vacuolar manganese by AtNRAMP3 and AtNRAMP4 is required for optimal photosynthesis and growth under manganese deficiency. Plant Physiol. 2010:**152**(4): 1986–1999. https://doi.org/10.1104/pp.109.150946

Lei Y, Korpelainen H, Li C. Physiological and biochemical responses to high Mn concentrations in two contrasting *Populus cathayana* populations. Chemosphere. 2007:**68**(4):686–694. https://doi.org/10.1016/j.chemosphere.2007.01.066

Lešková A, Giehl RFH, Hartmann A, Fargašová A, von Wirén N. Heavy metals induce iron deficiency responses at different hierarchic and regulatory levels. Plant Physiol. 2017:**174**(3):1648–1668. https://doi.org/10.1104/pp.16.01916

Liang HZ, Zhu F, Wang RJ, Huang XH, Chu JJ. Photosystem II of *Ligustrum lucidum* in response to different levels of manganese exposure. Sci Rep. 2019:**9**(1):12568. https://doi.org/10.1038/s41598-019-48735-8

Liu K, Yu F, Chen M, Zhou Z, Chen C, Li MS, Zhu J. A newly found manganese hyperaccumulator – *Polygonum lapathifolium* Linn. Int J Phytoremediation. 2016:**18**(4):348–353. https://doi.org/10.1080/15226514.2015.1109589

Liu T, Zhu L, Zhang Z, Huang H, Zhang Z, Jiang L. Protective role of trehalose and heavy metal stress in *Aureobasidium subglaciale* F134. Sci Rep. 2017:**7**(1):1–9. https://doi.org/10.1038/s41598-017-15489-0

Marschner H. Mineral nutrition of higher plants. Ann Bot. 1995:**78**(4): 527–528. https://doi.org/10.1006/anbo.1996.0155

Mengel K, Kirkby EA. Principles of plant nutrition. Ann Bot. 1987:**93**(4): 479–480. https://doi.org/10.1093/aob/mch063

Mercer FV, Nittim M, Possigham JV. The effect of manganese deficiency on the structure of spinach chloroplasts. J Cell Biol. 1962:**15**(2):379–381. https://doi.org/10.1083/jcb.15.2.379

Millaleo R, Reyes-Díaz M, Alberdi M, Ivanov AG, Krol M, Hüner NP. Excess manganese differentially inhibits photosystem I versus II in *Arabidopsis thaliana*. J Exp Bot. 2013:**64**(1):343–354. https://doi.org/10.1093/jxb/ers339

Millaleo R, Reyes-Diaz M, Ivanov AG, Mora ML, Alberdi M. Manganese as essential and toxic element for plants: transport, accumulation and resistance mechanisms. J Plant Nutr Soil Sci. 2010:**10**(4):470–481. https://doi.org/10.4067/S0718-95162010000200008

Molins H, Michelet L, Lanquar V, Agorio A, Giraudat J, Roach T, Krieger-Liszkay A, Thomine S. Mutants impaired in vacuolar metal mobilization identify chloroplasts as a target for cadmium hypersensitivity in *Arabidopsis thaliana*. Plant Cell Environ. 2013:**36**(4): 804–817. https://doi.org/10.1111/pce.12016

Nable RO, Houtz RL, Cheniae GM. Early inhibition of photosynthesis during development of Mn toxicity in tobacco. Plant Physiol. 1988:**86**(4):1136–1142. https://doi.org/10.1104/pp.86.4.1136

Nishiyama Y, Allakhverdiev SI, Murata N. Protein synthesis is the primary target of reactive oxygen species in the photoinhibition of photosystem II. Physiol Plant. 2011:**142**(1):35–46. https://doi.org/10.1111/j.1399-3054.2011.01457.x

Peiter E, Montanini B, Gobert A, Pedas P, Husted S, Maathuis FJ, Blaudez D, Chalot M, Sanders D. A secretory pathway-localized cation diffusion facilitator confers plant manganese tolerance. Proc Natl Acad Sci U S A. 2007:**104**(20):8532–8537. https://doi.org/10.1073/pnas.0609507104

Pittman JK. Managing the manganese: molecular mechanisms of manganese transport and homeostasis. New Phytol. 2005:**167**(3): 733–742. https://doi.org/10.1111/j.1469-8137.2005.01453.x

Porra RJ, Scheer H. Towards a more accurate future for chlorophyll a and b determinations: the inaccuracies of Daniel Arnon's assay. Photosynth Res. 2019:**140**(2):215–219. https://doi.org/10.1007/s11120-018-0579-8

Requena L, Bornemann S. Barley (*Hordeum vulgare*) oxalate oxidase is a manganese-containing enzyme. Biochem J. 1999:**343**(1):185–190. https://doi.org/10.1042/bj3430185

Salomon E, Keren N. Manganese limitation induces changes in the activity and in the organization of photosynthetic complexes in the cyanobacterium *Synechocystis* sp. strain PCC 6803. Plant Physiol. 2011:**155**(1):571–579. https://doi.org/10.1104/pp.110.164269

Samecka-Cymerman A, Marczonek A, Kempers AJ. Bioindication of heavy metals in soil by liverworts. Arch Environ Contam Toxicol. 1997:**33**(2):162–171. https://doi.org/10.1007/s002449900238

Satoh K, Butler WL. Low temperature spectral properties of subchloroplast fractions purified from spinach. Plant Physiol. 1978:**61**(3): 373–379. https://doi.org/10.1104/pp.61.3.373

Schaffner W, Weissmann C. A rapid, sensitive, and specific method for the determination of protein in dilute solution. Anal Biochem. 1973:**56**(2):502–514. https://doi.org/10.1016/0003-2697(73)90217-0

Schmidt SB, Jensen PE, Husted S. Manganese deficiency in plants: the impact on photosystem II. Trends Plant Sci. 2016:**21**(7):622–632. https://doi.org/10.1016/j.tplants.2016.03.001

Sharma SS, Dietz K-J. The significance of amino acids and amino acid-derived molecules in plant responses and adaptation to heavy metal stress. J Exp Bot. 2006:**57**(4):711–726. https://doi.org/10.1093/jxb/erj073

Shimakawa G, Hanawa H, Wada S, Hanke GT, Matsuda Y, Miyake C. Physiological roles of flavodiiron proteins and photorespiration in the liverwort *Marchantia polymorpha*. Front Plant Sci. 2021:**19**(12): 668805. https://doi.org/10.3389/fpls.2021.668805

Singh S, Parihar P, Singh R, Singh VP, Prasad SM. Heavy metal tolerance in plants: role of transcriptomics, proteomics, metabolomics, and ionomics. Front Plant Sci. 2016:**8**:1143. https://doi.org/10.3389/fpls.2015.01143

St. Clair SB, Lynch JP. Differences in the success of sugar maple and red maple seedlings on acid soils are influenced by nutrient dynamics and light environment. Plant. Cell Environ. 2005:**28**(7):874–885. https://doi.org/10.1111/j.1365-3040.2005.01337.x

Strasser BJ. Donor side capacity of photosystem II probed by chlorophyll a fluorescence transients. Photosynth Res. 1997:**52**(2): 147–155. https://doi.org/10.1023/A:1005896029778

Streckaite S. Thylakoids: from molecular to membrane organisation. A spectroscopic and nanoscopic study of the photosynthetic apparatus [PhD thesis]. [Amsterdam]: Vrije Universiteit Amsterdam; 2021.

Subrahmanyam D, Rathore VS. Influence of manganese toxicity on photosynthesis in ricebean (*Vigna umbellata*) seedlings. Photosynthetica. 2001:**38**(3):449–453. https://doi.org/10.1023/A:1010998226323

Tanaka H, Sato M, Ogasawara Y, Hamashima N, Buchner O, Holzinger A, Toyooka K, Kodama Y. Chloroplast aggregation during the cold-positioning response in the liverwort *Marchantia polymorpha*. J Plant Res. 2017:**130**(6):1061–1070. https://doi.org/10.1007/s10265-017-0958-9

Van der Ent A, Baker AJM, Reeves RD, Pollard AJ, Schat H. Hyperaccumulators of metal and metalloid trace elements: facts and fiction. Plant Soil. 2013:**362**(1–2):319–334. https://doi.org/10.1007/s11104-012-1287-3

Vert G, Grotz N, Dédaldechamp F, Gaymard F, Guerinot ML, Briat JF, Curie C. IRT1, an Arabidopsis transporter essential for iron uptake from the soil and for plant growth. Plant Cell. 2002:**14**(6):1223–1233. https://doi.org/10.1105/tpc.001388

Zhang B, Zhang C, Liu C, Jing Y, Wang Y, Jin L, Yang L, Fu A, Shi J, Zhao F, et al. Inner envelope CHLOROPLAST MANGANESE TRANSPORTER 1 supports manganese homeostasis and phototrophic growth in Arabidopsis. Mol Plant. 2018:**11**(7):943–954. https://doi.org/10.1016/j.molp.2018.04.007